A Ritz Model for Damage Analysis in Variable Angle Tow Composite Plates

Dario Campagna,[1, a)] Vincenzo Oliveri,[2, b)] Alberto Milazzo,[1, c)] and Ivano Benedetti[1, d)]

[1)] *Department of Engineering, University of Palermo, Viale delle Scienze, Edificio 8, 90128, Palermo, Italy.*
[2)] *School of Engineering and Bernal Institute, University of Limerick, V94 T9PX, Limerick, Ireland.*

[a)] *Electronic mail: dario.campagna@unipa.it*
[b)] *Electronic mail: vincenzo.oliveri@ul.ie*
[c)] *Electronic mail: alberto.milazzo@unipa.it*
[d)] *Corresponding author: ivano.benedetti@unipa.it*

Abstract. In this work, a Ritz method is developed for progressive damage analysis of multilayered variable angle tow (VAT) composite plates under geometrically non-linear strains. The proposed model adopts a first order shear deformation theory and considers geometric non-linearities through the von Karman assumptions. A meso-modelling approach based on Continuum Damage Mechanics is adopted for analysing the initiation and evolution of damage. The onset of damage is predicted using the Hashin's criteria. Four damage indices are defined and computed for expressing the degradation of the mechanical properties of the material, both for fibers and matrix under either tension and compression loading. A set of numerical tests is carried out to validate the model, assess its convergence and show its capabilities, eventually presenting novel results for progressive non-linear damage in variable angle tow composite plates.

INTRODUCTION

Multilayered composite materials are widely employed in several field of engineering, such as aerospace, naval and automotive, as they allow the design of low-weight structures with enhanced stiffness, strength and fatigue properties, among others. Thanks to the availability of new manufacturing techniques, such as automated fibre placement, automated tape laying and additive manufacturing, composite structures can be designed and produced with variable mechanical properties, so as to realize the so called variable angle tow (VAT) laminates, obtained by varying the fibre orientation as a function of the position considered over the structure. The advantages offered by VAT laminates are nowadays well-known and have been extensively studied [1, 2, 3].

Besides developing new manufacturing techniques for the production of advanced materials and structural components, engineers need computational modelling tools able to predict the structural response of the designed components; considering the width of the materials design space allowed by the mentioned novel manufacturing techniques, the availability of effective computational tools provides an asset that may help noticeably reduce experimental times and costs, thus contributing to unleash the higher potential of new manufacturing/materials routes.

One of the most employed numerical approaches to structural problems is the Finite Element Method (FEM), which has also reached a well definite maturity. FEM's accuracy is strongly related to the suitable quality of the generated mesh that, in the case of VAT laminates, due to the variation of the in-plane and through-the-thickness properties, generally indices a high number of mesh elements, thus leading to high computational efforts [4, 5]. To overcome such issues, and possibly speed up the analysis still retaining a high level of accuracy, different numerical techniques have been proposed as alternative to FEM, such as boundary elements methods [6, 7, 8] or mesh-less techniques [9]; in this context, the Ritz method, which may be seen as a global mesh-less technique, has been often shown effective for the analysis of classical, laminated and VAT composite structures [10, 11, 12, 13].

To fully exploit the advantages offered by VAT composites, and identify their operational domain, it is important to assess and possibly predict the onset and evolution of damage, as done for other engineering materials and classical straight-fiber laminates. Different approaches have been used to model the initiation and evolution of damage in composite structures. Depending on the scale of the idealization, from microscale through mesoscale to macroscale, damage can be modelled in different ways.

At the microscale, micromechanical approaches are generally used where the evolution of damage is represented either in the form of matrix softening or fibers breaking, being both the matrix and the fibers explicitly represented in the so called representative volume element (RVE) [14, 15, 16, 17]. Such approaches are typically used for representing the mechanical response before cracks localize at ply level or at the larger scale. At the opposite macroscale or component level, the damage is often represented as a hard discontinuity, e.g. a crack or concentrated reduction of material stiffness. At the mesoscale, where the individual plies are represented as homogenous, at least through the thickness, the damage process can be treated using different theories. One of the most common is the Continuum Damage Mechanics (CDM). CDM models are based on the works done by Matzenmiller and Ladeveze among others [18, 19], where damage is represented as a progressive reduction of material stiffness. CDM has also been employed to model damage in nano-mechanics [20] and multiscale applications [21].

Within the CDM framework, different FEM models have been developed for investigating the initiation and development of damage in composites. Maimí et al. [22, 23] developed a CDM-FE model for the prediction of the onset and evolution of intralaminar failure mechanisms with a damage activation functions based on the LaRC04 failure criteria. Ferreira et al. [24] developed a higher-order FE model considering progressive damage in a structural formulation based on a generalised kinematics. Lopes and coworkers [25] employed a user-developed continuum damage model implemented in the commercial FE software ABAQUS for the analysis of progressive damage in post-buckling up to structural failure due to accumulation of fibre and matrix damage for VAT composite laminates.

Few works have been devoted to the development of Ritz approaches to the analysis of progressive damage in straight-fibers composite laminates. Yang and Hayman [26, 27] developed a semi-analytical method for estimating the ultimate strength of rectangular composite laminates subjected to uniaxial in-plane compression using both an instantaneous and a linear degradation model.

To the best of the authors' knowledge, the progressive damage behaviour of VAT composite laminates using the Ritz approach still remains unexplored.

FORMULATION OVERVIEW

In this section, the key items of the formulation are briefly discussed.

Kinematics and strain-displacement relationships

The model kinematics is based on the First order Shear Deformation Theory (FSDT). Referring to a Cartesian coordinate system $x_1x_2x_3$ with the x_3 axis directed along the thickness, the displacements are given by

$$\boldsymbol{d} = \boldsymbol{u} + x_3\boldsymbol{L}\boldsymbol{\vartheta} + \bar{\boldsymbol{w}}, \tag{1}$$

where

$$\boldsymbol{L} = \begin{bmatrix} 1 & 0 & 0 \\ 0 & 1 & 0 \end{bmatrix}^T. \tag{2}$$

In Eq.(1), the vectors $\boldsymbol{u}$ and $\boldsymbol{\vartheta}$ collect the reference plane displacement components and the section rotations, respectively, and the vector $\bar{\boldsymbol{w}}$ collects an initial prescribed imperfection, namely

$$\boldsymbol{u} = \{u_1, u_2, u_3\}^T \qquad \boldsymbol{\vartheta} = \{\vartheta_1, \vartheta_2\}^T \qquad \bar{\boldsymbol{w}} = \{0, 0, \bar{w}\}^T. \tag{3}$$

In the framework of large displacements, assuming geometric non-linearity in the von-Karman sense, the strain-displacement relationships are written as [10]

$$\boldsymbol{e}_p = \begin{Bmatrix} e_{11} \\ e_{22} \\ e_{12} \end{Bmatrix} = \boldsymbol{\mathcal{D}}_p \boldsymbol{u} + \frac{1}{2} \left(\boldsymbol{\mathcal{D}}_p \otimes u_3 \right) \boldsymbol{\mathcal{D}}_n \boldsymbol{u} + x_3 \boldsymbol{\mathcal{D}}_p \boldsymbol{L} \boldsymbol{\vartheta} + \left(\boldsymbol{\mathcal{D}}_p \otimes \bar{w} \right) \boldsymbol{\mathcal{D}}_n \boldsymbol{u} = \\ = \boldsymbol{\varepsilon}_p + \boldsymbol{\varepsilon}_{nl} + x_3 \boldsymbol{\kappa} + \bar{\boldsymbol{\varepsilon}} = \\ = \boldsymbol{\varepsilon}_0 + x_3 \boldsymbol{\kappa} \tag{4}$$

and

$$\boldsymbol{e}_n = \begin{Bmatrix} e_{13} \\ e_{23} \\ e_{33} \end{Bmatrix} = \boldsymbol{\mathcal{D}}_n \boldsymbol{u} + \boldsymbol{L} \boldsymbol{\vartheta} = \boldsymbol{\gamma} \tag{5}$$

where $\boldsymbol{\mathcal{D}}_p$ and $\boldsymbol{\mathcal{D}}_n$ are defined as

$$\boldsymbol{\mathcal{D}}_p = \begin{bmatrix} \frac{\partial}{\partial x} & 0 & 0 \\ 0 & \frac{\partial}{\partial y} & 0 \\ \frac{\partial}{\partial y} & \frac{\partial}{\partial x} & 0 \end{bmatrix} \qquad \boldsymbol{\mathcal{D}}_n = \begin{bmatrix} 0 & 0 & \frac{\partial}{\partial x} \\ 0 & 0 & \frac{\partial}{\partial y} \\ 0 & 0 & 0 \end{bmatrix} \tag{6}$$

Constitutive relations

For the k-th lamina, the following relations hold

$$\boldsymbol{\sigma}_p = \boldsymbol{Q}_p \boldsymbol{e}_p \qquad \boldsymbol{\sigma}_n = \boldsymbol{Q}_n \boldsymbol{e}_n. \tag{7}$$

In Eq.(7), the matrices $\boldsymbol{Q}_p$ and $\boldsymbol{Q}_n$ depend on the local fiber orientation for each ply. Moreover, the in plane stiffness coefficient are function of the evolution of the damage. The generic damaged in-plane stiffness matrix in the orthotropic material reference system reads as [18]

$$\boldsymbol{C} = \frac{1}{D} \begin{bmatrix} (1-\omega_1)E_1 & (1-\omega_1)(1-\omega_2)\nu_{21}E_1 & 0 \\ (1-\omega_1)(1-\omega_2)\nu_{21}E_2 & (1-\omega_2)E_2 & 0 \\ 0 & 0 & D(1-\omega_6)G_{12} \end{bmatrix} \tag{8}$$

with $D = 1 - (1-\omega_1)(1-\omega_2)\nu_{12}\nu_{21}$. In Eq.(8), ω_1, ω_2 and ω_6 are the longitudinal (fiber–dominated) transverse (matrix–matrix–dominated) and shear damage indices respectively.

Damage onset and evolution

In the present model, an activation criterion to identify the damage onset is used. After a failure threshold is overcome, the corresponding damage index will follow an evolution law, thus inducing strain softening in the constitutive material response. The adopted activation criteria are based on the Hashin's theory [28, 29].

After the onset of damage, an increase in load will cause the evolution of the activated damage indices and the degradation of the associated material properties. Referring to a linear softening law, shown in Fig.(1), a damage index is compute as follows

$$\omega_i = \frac{e_{i,eq}^f \left(e_{i,eq} - e_{i,eq}^0 \right)}{e_{i,eq} \left(e_{i,eq}^f - e_{i,eq}^0 \right)} \qquad i = ft, fc, mt, mc \tag{9}$$

where $e^0_{i,eq}$ is the equivalent strain at damage onset and $e^f_{i,eq} = \alpha e^0_{i,eq}$ is the equivalent strain upon rupture. The equivalent strains are computed for each damage mode as follows

$$e_{ft,eq} = \langle e_{11} \rangle \qquad e_{fc,eq} = \langle -e_{11} \rangle \tag{10}$$

$$e_{mt,eq} = \sqrt{\langle e_{22} \rangle^2 + e_{12}^2} \qquad e_{mc,eq} = \sqrt{\langle -e_{22} \rangle^2 + e_{12}^2} \tag{11}$$

where $\langle \bullet \rangle = (\bullet + | \bullet |)/2$ denote the Macaulay brackets.

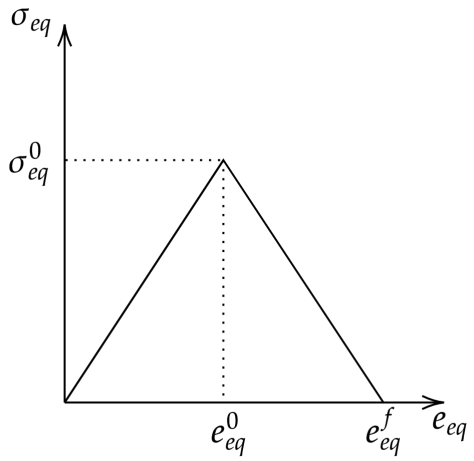

FIGURE 1. Stress-strain softening curve.

Governing equations

The problem governing equation are obtained enforcing the stationarity of the structural total energy. By adopting a Ritz approximation with orthogonal polynomials based trial functions and according with reference [10], the structural governing equation are obtained and may be written in compact notation as

$$\left\{ \boldsymbol{K}_0 + \bar{\boldsymbol{K}}_0 + \boldsymbol{K}_1 + \boldsymbol{K}_2 + \bar{\boldsymbol{K}}_1 + \boldsymbol{R} \right\} \boldsymbol{X} = \boldsymbol{F}_D + \boldsymbol{F}_L \tag{12}$$

where $\boldsymbol{K}_0, \boldsymbol{K}_1, \boldsymbol{K}_2, \bar{\boldsymbol{K}}_0, \bar{\boldsymbol{K}}_1$ are the stiffness matrices in which the subscripts 1,2 refer to the geometric non-linear terms and the overbar refers to the prescribed initial imperfection. Moreover, $\boldsymbol{R}$ is the matrix used to enforce the BCs thorough a penalty approach and $\boldsymbol{X}$ is the vector collecting the unknown coefficient of the Ritz series expansion. On the right hand side, the vectors $\boldsymbol{F}_D$ and $\boldsymbol{F}_L$ collect the external loads. Further details may be found in Ref. [10].

Incremental form

To solve the non-linear damage problem an incremental-iterative procedure is used. Noting that all the matrices on the left hand side of Eq.(12) except $\boldsymbol{R}$ depend on the solution vector $\boldsymbol{X}$, the differentiation of the governing equations leads to the incremental expression

$$\boldsymbol{R}\,\Delta\boldsymbol{X} + \Delta\left\{ \left[\boldsymbol{K}_0 + \bar{\boldsymbol{K}}_0 + \boldsymbol{K}_1 + \boldsymbol{K}_2 + \bar{\boldsymbol{K}}_1 \right] \boldsymbol{X} \right\} = \Delta\boldsymbol{F}_D + \Delta\boldsymbol{F}_L \tag{13}$$

where

$$\Delta\left\{ \boldsymbol{K}_0 \boldsymbol{X} \right\} = \left(\boldsymbol{K}_0 + \frac{\partial \boldsymbol{K}_0}{\partial \omega_i} \frac{\partial \omega_i}{\partial \boldsymbol{e}_p} \frac{\partial \boldsymbol{e}_p}{\partial \boldsymbol{X}} \boldsymbol{X} \right) \Delta\boldsymbol{X} = \left(\boldsymbol{K}_0 + \boldsymbol{K}_{0D} \right) \Delta\boldsymbol{X} \tag{14}$$

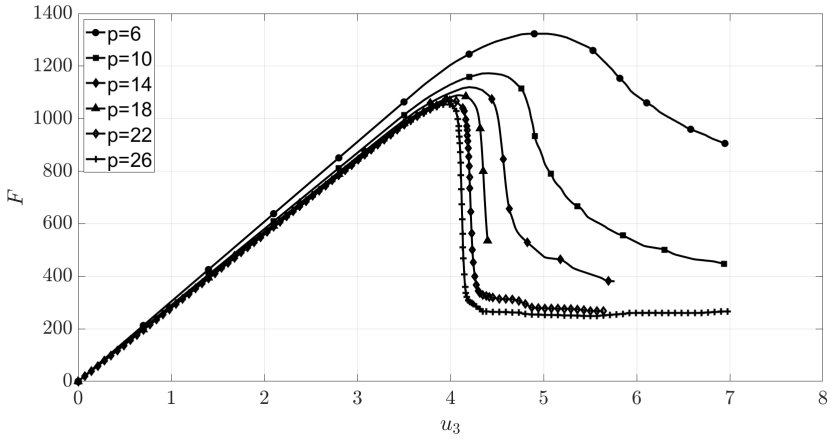

FIGURE 2. Convergence study for the three-point bending test of the unidirectional laminate.

and

$$\Delta\left[\left(\boldsymbol{K}_1+\boldsymbol{K}_2+\bar{\boldsymbol{K}}_0+\bar{\boldsymbol{K}}_1\right)\boldsymbol{X}\right]=\left(\boldsymbol{K}_{1t}+\boldsymbol{K}_{2t}+\bar{\boldsymbol{K}}_{1t}+\boldsymbol{K}_G+\boldsymbol{K}_{12D}\right)\Delta\boldsymbol{X} \tag{15}$$

where $\boldsymbol{K}_{1t}$, $\boldsymbol{K}_{2t}$,$\bar{\boldsymbol{K}}_{1t}$ and $\boldsymbol{K}_G$ are the tangent stiffness terms related to the geometric non-linearities and the initial imperfections, while $\boldsymbol{K}_{0D}$ and $\boldsymbol{K}_{12D}$ are the tangent stiffness terms related to the damage evolution.

NUMERICAL RESULTS

Convergence analysis and validation

The composite plate used in the first case study is a unidirectional laminate $[0]_{10}$ with a total thickness $t = 1.8\,\text{mm}$, made of carbon fiber/epoxy M10. The material properties, listed in Table I, are taken from Ref. [30]. The composite plate has size $60 \times 25\,\text{mm}^2$, and undergoes a three point bending test loading.

TABLE I. Material properties of straight fiber lamina.

Elastic property	Value	Strenght property	Value
E_1	105.00 GPa	X_T	1400.0 MPa
E_2	8.57 GPa	X_C	930.0 MPa
G_{12}	4.39 GPa	Y_T	47.0 MPa
$G_{23} = G_{13}$	3.05 GPa	Y_C	60.3 MPa
ν_{12}	0.34	S_L	53.0 MPa

First, a convergence study is carried out. As it can be seen from Fig.(2) for this particular case a high number of polynomials has to be used in order to achieve convergence. The obtained results have been compared with experimental measurements and with the results obtained from FE modelling [24]. As it can be observed in Fig.(3), even if the proposed model underestimate the maximum load, it provides good agreement with the experimental test measurements.

VAT composite plate

After validation, the developed method has been used to study the post-buckling behavior of a VAT laminate that undergoes a compression load. The plate stacking sequence is $[0 \pm \langle 0|45\rangle]_{4S}$ (the notation proposed

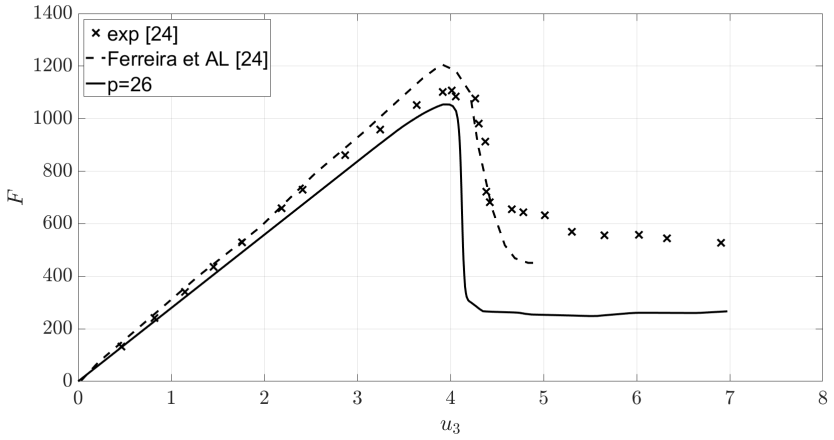

FIGURE 3. Comparison between the present model, experimental results and FEM results for the three-point bending test of the unidirectional laminate.

in Ref. [11] is adopted for VAT laminae description) with a total thickness $t = 6.25\,\text{mm}$ and dimensions of $250 \times 250\,\text{mm}^2$. The material properties of each lamina are listed in Tab.II. Fig.(4) reports the comparison between the responses provided by the present model, with and without progressive damage model activation, in terms of applied in-plane force and out of plane deflection of plate's center point. It is observed that in the post-buckling regime after the damage onset the load capabilities of the plate change significantly, denoting the importance of taking into account the onset and the evolution of damage in composite structures.

TABLE II. Material properties for a VAT lamina.

Elastic property	Value	Strenght property	Value
E_1	163.00 GPa	X_T	2034 MPa
E_2	6.80 GPa	X_C	1234 MPa
$G_{12} = G_{23} = G_{13}$	3.40 GPa	Y_T	927 MPa
ν_{12}	0.34	Y_C	176 MPa
		S_L	186 MPa

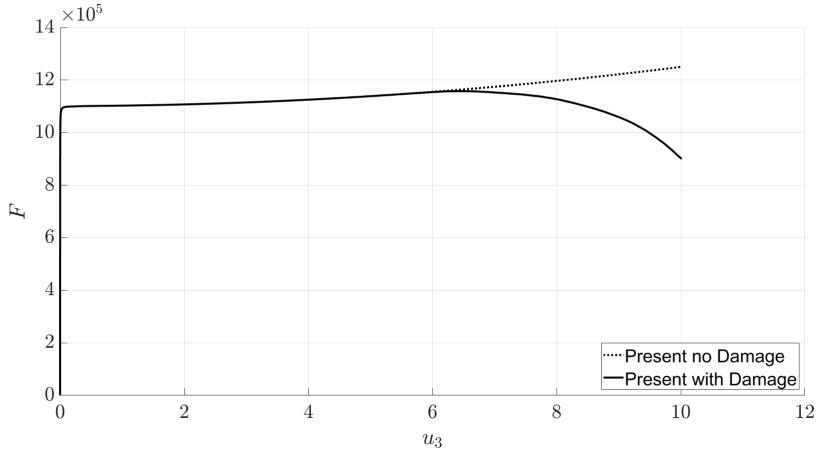

FIGURE 4. Comparison of force-displacement results with and without damage for VAT laminates under compression load.

The formulation is currently being extended to the study of impact-induced damage in VAT laminated plates [31].

CONCLUSIONS

In this work, a Ritz approach for modelling the progressive failure of VAT composite plates either in linear or post-buckling regime has been developed.

The method adopts the first order shear deformation theory with non-linear von Karman strains assumptions for representing geometrically non-linear deformations and a continuum damage mechanics approach at the meso-scale for capturing the initiation and evolution of damage. Damage initiation is triggered according to a Hashin's failure criteria. The developed model has been implemented and successfully validated against available data provided by either FE damage models or experimental tests. Some preliminary results have been reported for post-buckling analysis of composite VAT laminated plates in presence of damage. Further tests are being performed to assess the performance and robustness of the proposed method and to extend its capability to the analysis of impact-induced damage in composite plates.

ACKNOWLEDGMENTS

The Authors gratefully acknowledge the support of the PON Ricerca e Innovazione 2014-2020 – Fondo Sociale Europeo, Azione I.1 "Dottorati Innovativi con caratterizzazione Industriale" – Ciclo XXXVI (CUP: B73D20005010001 – Scholarship ID: DOT20KTEXX).

REFERENCES

1. Z. Gurdal and R. Olmedo, AIAA J. **31**, 751–758 (1993).
2. Z. Gürdal, B. Tatting, and C. Wu, Compos. A Appl. Sci. Manuf. **39**, 911–922 (2008).
3. Z. Wu, P. M. Weaver, G. Raju, and B. Chul Kim, Thin-Walled Struct. **60**, 163–172 (2012).
4. L. Demasi, G. Biagini, F. Vannucci, E. Santarpia, and R. Cavallaro, Compos. Struct. **177**, 54–79 (2017).
5. V. Gulizzi, I. Benedetti, and A. Milazzo, Mech. Adv. Matl. Struct. **27**, 1494–1508 (2020).
6. I. Benedetti, M. Aliabadi, and G. Davì, Int. J. Solids. Struct. **45**, 2355–2376 (2008).
7. I. Benedetti and M. H. Aliabadi, Int. J. Numer. Meth. Eng. **84**, 1038–1067 (2010).
8. V. Gulizzi, I. Benedetti, and A. Milazzo, Theor. Appl. Fract. Mec. **104**, 102329 (2019).
9. K. Liew, X. Zhao, and A. J. Ferreira, Compos. Struct. **93**, 2031–2041 (2011).
10. A. Milazzo and V. Oliveri, AIAA J. **55**, 965–980 (2017).
11. V. Oliveri and A. Milazzo, Comput. Struct. **196**, 263–276 (2018).
12. A. Milazzo, I. Benedetti, and V. Gulizzi, Compos. Struct. **201**, 980–994 (2018).
13. A. Milazzo, I. Benedetti, and V. Gulizzi, Int. J. Solids. Struct. **159**, 221–231 (2019).
14. C. González and J. LLorca, Compos. Sci. Technol. **67**, 2795–2806 (2007).
15. M. Lo Cascio, A. Milazzo, and I. Benedetti, Compos. Struct. **232**, 111523 (2020).
16. M. Lo Cascio, A. Milazzo, and I. Benedetti, Int. J. Mech. Sci. **199**, 106404 (2021).
17. M. Lo Cascio and I. Benedetti, J. Multiscale Model. **13**, 2144001 (2022).
18. A. Matzenmiller, J. Lubliner, and R. Taylor, Mech. Mater. **20**, 125–152 (1995).
19. P. Ladeveze and E. LeDantec, Compos. Sci. Technol. **43**, 257–267 (1992).
20. I. Benedetti, H. Nguyen, R. A. Soler-Crespo, W. Gao, L. Mao, A. Ghasemi, J. Wen, S. Nguyen, and H. D. Espinosa, J. Mech. Phys. Solids **112**, 66–88 (2018).
21. I. Benedetti and M. Aliabadi, Comput. Methods Appl. Mech. Eng. **289**, 429–453 (2015).
22. P. Maimí, P. Camanho, J. Mayugo, and C. Dávila, Mech. Mater. **39**, 897–908 (2007).
23. P. Maimí, P. Camanho, J. Mayugo, and C. Dávila, Compos. A Appl. Sci. Manuf. **39**, 909 – 919 (2007).
24. G. F. Ferreira, J. H. S. Almeida, M. L. Ribeiro, A. J. Ferreira, and V. Tita, Thin-Walled Struct. **172**, 108864 (2022).
25. C. Lopes, P. Camanho, Z. Gürdal, and B. Tatting, Int. J. Solids. Struct. **44**, 8493–8516 (2007).
26. Q. J. Yang and B. Hayman, Compos. B. Eng. **69**, 13–21 (2015).
27. Q. J. Yang and B. Hayman, Eng. Struct. **84**, 42–53 (2015).
28. Z. Hashin and A. Rotem, J. Compos. Mater. **7**, 448–464 (1973).
29. Z. Hashin, J. Appl. Mech. **47**, 329–334 (1980).
30. V. Tita, J. de Carvalho, and D. Vandepitte, Compos. Struct. **83**, 413–428 (2008).
31. A. Milazzo and I. Benedetti, Compos. Struct. **276**, 114533 (2021).